Chapter 5
Langmuir-Type Model Analysis

In this chapter, based on the rigorous theory of anomalous diffusion through fibrous porous media (Langmuir-type model), its advantagens, limitations, and different approaches (analytical and numerical), we present the correct prediction for the water absorption process in vegetable fiber-reinforced polymer composites. In the macroscopic and advanced mathematical modeling, both fiber and polymer are considered a homogeneous mixture having water molecules in the free and entrapped states inside the material, and the effect of swelling is neglected. Herein, different 1D and 3D simulation results of the average moisture content, moisture content as well as free and entrapped water molecules concentration distribution at different times are presented and analyzed. Applications have been focused to caroá fiber- reinforced polyester composites and other arbitrary cases.

5.1 Fundamentals

The effects of moisture absorption on the physical and chemical properties of polymer composite materials have received wide attention, not only due to the durability of these materials in operation but also because of their wide field of application.

As already mentioned, the properties of composite materials depend on the behavior of the matrix, the reinforcement and the fiber/matrix interface. Absorption of water molecules in materials leads to degradation of the interface and swelling of the matrix, generating internal stresses and decreasing mechanical properties. Decreasing properties are intrinsically associated to the moisture diffusion process in composite materials and therefore, in order to predict long-term behavior, in-service failure and useful life estimation [1], it is essential to know the water absorption rate.

Diffusion models must reflect the moisture sorption process in different ways, considering certain additional phenomena that can occur inside the material. Thus,

J. M. P. Q. Delgado et al., *Moisture Transport in Polymer Composite Materials*,
Advanced Structured Materials 160, https://doi.org/10.1007/978-3-030-77826-2_5

each specific case must be analyzed not only based on the results of a good approximation between the experimental data and those predicted by the equations, but also by the physical interpretation of the water sorption process included in the models.

In some cases, the water absorption kinetics is described assuming that water absorption follows the classical treatment given by Fick's second law of diffusion, that is, that the diffusion process is driven by the water concentration gradient between the medium and the material and continues until hygroscopic equilibrium is reached. In others, this model is not well suited [2, 3], because the material presents an anomalous water diffusion behavior, which implies in the existence of different stages of sorption until the final mass balance is reached (hygroscopic equilibrium condition). In this case, single-phase models cannot easily describe this kind of diffusion, and one needs other more sophisticated models to describe the behavior of the material under these physical conditions [4]. The Langmuir-type model is appropriate to predict the non-Fickian diffusion process in this situation [5].

The Langmuir-type model explains moisture sorption by assuming that water exists simultaneously in two phases: free (unbound) and entrapped (bound), during the process. In this model, water molecules in the free phase are adsorbed (bound) with a probability α per unit time, and the entrapped water molecules can leave the connected state with a probability β per unit time. Thus, the diffusion process is described by the classical diffusion equation, which is modified to take into account the two phases of the moisture inside the material.

Figure 5.1 illustrates the moisture content transient behavior predicted by Fick´s model and Langmuir-type model. According to the Langmuir-type model, during the water absortion process, moisture migration is controlled by two phenomena: dispersion of free water molecules due to random molecular motion and trapping of water molecules due to interaction between the free water molecules and porous within the polymer composite.

In Fig. 5.1, the pseudo-equilibrium point represents the point at which the moisture migration rate drops dramatically.

The Langmuir-type model is well described in Glaskova et al. [6], Carter and Kilber [5], Bonniau and Bunsell [1], Grace and Altan [2], Cotinaud et al. [7] and Apicella et al. [8].

According to Carter and Kilber [5], the diffusive characteristics of the Langmuir-type model are correlated to the simplest form of neutron transport theory, while that the characteristics associated to free and entrapped water molecules are related to the classical Langmuir´s adsorption isotherms theory.

According to these authors, composite anisotropy (structural heterogeneity), swelling, size and distribution of micropores (microvoids), mechanical loading, rearrangement of the polymer network (long-term relaxation), or some other phenomenon not yet fully understood are responsible for the intensity of the physical or chemical interactions at the microscopic level between polar water molecules and molecular groups of the polymer chains (molecular binding). A detailed discussion on the applications of this model are presented in the next section.

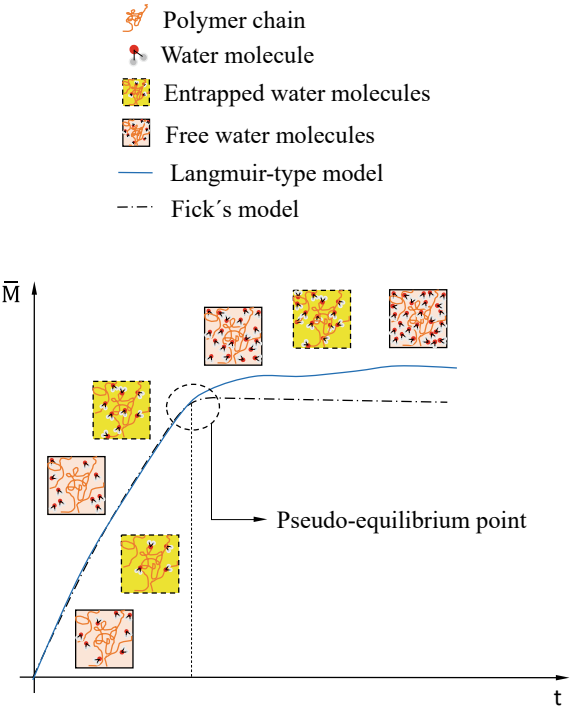

Fig. 5.1 Typical moisture absorption kinetics predicted by Langmuir-type model and Fick´s model

5.2 Moisture Absorption by Langmuir-Type Model

5.2.1 The Physical Problem

For the analysis of the physical problem studied here, consider a dry polymer composite of parallelepiped geometry, at low temperature, suddenly immersed in a stationary, heated, saturated fluid (water). As the surrounding fluid heats the dry porous media, heat penetrates into the solid (as the result of a temperature difference) and moisture migrates into the solid by diffusion from the surface. Figure 5.2 illustrates the problem treated here. In this figure Lx, Ly, and Lz are the distances from the composite surface to the maximum level of water in the container.

5.2.2 The General Mass Diffusion Equation

In the Langmuir-type model, the non-Fickian moisture absorption behavior can be explained quantitatively by assuming that moisture absorption occurs in the presence of two simultaneous stages, one being the free water stage and the another the entrapped water stage [5]. The following mass transfer equations describe this model:

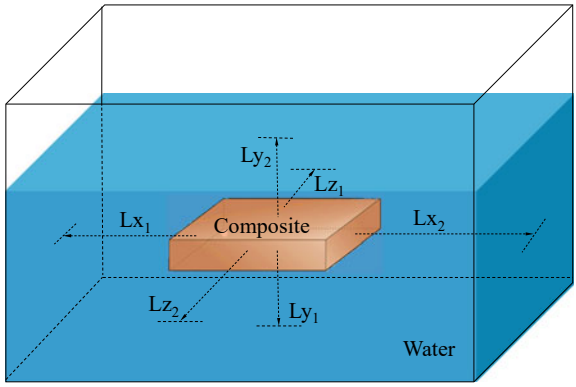

Fig. 5.2 Squematic of the composite immersed in a stationary fluid and the distance of the material to borders of the fluid domain

$$\frac{\partial C}{\partial t} = \nabla \cdot (D \nabla C) - \frac{\partial S}{\partial t} \tag{5.1}$$

$$\frac{\partial S}{\partial t} = \lambda C - \mu S \tag{5.2}$$

where: C is the concentration of the free solute diffusing into the material; S is the concentration of the entrapped solute; D is the mass diffusion coefficient (free solute molecules); t is the time; λ is the probability of a free solute molecule is entrapped inside the solid and μ is the probability that an entrapped solute molecule becomes free.

Careful analysis of Eq. (5.1), indicates that if $\lambda = 0$ or $\mu >> \lambda$, it is reduced to the simple diffusion theory (Fick´s second law of diffusion).

5.2.3 *The Mass Diffusion Equation: 3D Approach in Cartesian Coordinates*

For a three-dimensional and transient approach, based on the considerations adopted, the Langmuir model, in Cartesian Coordinates, can be written as:

$$\frac{\partial C}{\partial t} = \frac{\partial}{\partial x}\left(D \frac{\partial C}{\partial x}\right) + \frac{\partial}{\partial y}\left(D \frac{\partial C}{\partial y}\right) + \frac{\partial}{\partial z}\left(D \frac{\partial C}{\partial z}\right) - \frac{\partial S}{\partial t} \tag{5.3}$$

$$\frac{\partial S}{\partial t} = \lambda C - \mu S \tag{5.4}$$

In order to solve Eqs. 5.3 and 5.4, the following initial and boundary conditions were used:

(a) ***Initial conditions***: if the solid is completely dry at the beginning of the process, then one can write:

$$C = S = 0; \begin{cases} -R_1 < x < R_1 \\ -R_2 < y < R_2 \\ -R_3 < z < R_3 \end{cases} \tag{5.5}$$

(b) ***Boundary conditions:*** the variation in the concentration of the solute in the fluid medium on the surface of the solid is equal to the diffusive flux of solute into the material. Then, one can write:

$$Lx_1 \frac{\partial C}{\partial t} = -D \frac{\partial C}{\partial x}; \begin{cases} x = -R_1 \\ t > 0 \end{cases} \tag{5.6}$$

$$Lx_2 \frac{\partial C}{\partial t} = -D \frac{\partial C}{\partial x}; \begin{cases} x = +R_1 \\ t > 0 \end{cases} \tag{5.7}$$

$$Ly_1 \frac{\partial C}{\partial t} = -D \frac{\partial C}{\partial y}; \begin{cases} x = -R_2 \\ t > 0 \end{cases} \tag{5.8}$$

$$Ly_2 \frac{\partial C}{\partial t} = -D \frac{\partial C}{\partial y}; \begin{cases} x = +R_2 \\ t > 0 \end{cases} \tag{5.9}$$

$$Lz_1 \frac{\partial C}{\partial t} = -D \frac{\partial C}{\partial z}; \begin{cases} x = -R_3 \\ t > 0 \end{cases} \tag{5.10}$$

$$Lz_2 \frac{\partial C}{\partial t} = -D \frac{\partial C}{\partial z}; \begin{cases} x = +R_3 \\ t > 0 \end{cases} \tag{5.11}$$

Once C and S are determined at any point inside the material, it is possible to calculate the total moisture content present in the material at any position and instant of time. Therefore, the total moisture content is given by the sum of the concentrations of C and S, as follows:

$$M(x,y,z,t) = C(x,y,z,t) + S(x,y,z,t) \tag{5.12}$$

It follows from Eq. 5.12 that the average moisture content of the solid at any time of the process is given by:

$$\overline{M} = \frac{1}{V} \int_V M(x,y,z,t) dV \tag{5.13}$$

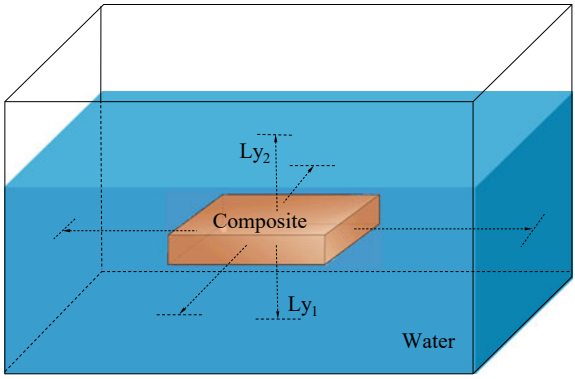

Fig. 5.3 Geometrical representation of the one-dimensional physical problem

in which V is the total volume of the solid and dV = dxdydz is the volume of an infinitesimal sample of the porous solid.

5.2.4 The Water Absorption Process: 1D Approach in Cartesian Coordinates

5.2.4.1 The Physical Problem

For the physical model, a porous plate with thickness $2R_2 = 2a$, immersed in a fluid solution (water) of height $(Ly_1 + 2a + Ly_2)$, as illustrated in Fig. 5.3 was considered.

Considering that $R_1 = R_3 >> R_2$, water absorption can be analysed just in the y direction and the following assumptions were made: the material is homogeneous and isotropic; the mass diffusion coefficient is constant; the solid is axisymmetric; the process is transient; the dimensions of the material during the diffusion process do not change; the capillary transport through the solid is negligible; mass generation inside the solid is neglected; the solid is totally dry at the beginning of the process and the solid is in equilibrium with the surrounding medium at the surface (equilibrium boundary condition).

5.2.4.2 The Mass Diffusion Equation

In the Langmuir-Type model, the anomalous moisture absorption can be quantitatively determined by assuming that absorbed moisture consists of a mobile phase and a bound phase. The model considers the interaction between the polar water molecules and the resin molecular groups, predicting the existence of free and bound molecules within the polymer network. This can be taken into account by adding a new parameter to the classical Fick's equation [9]. Considering the assumptions already cited, the Langmuir equation, written in Cartesian coordinates in a one-dimensional approach, is described as follows:

$$\frac{\partial C}{\partial t} = D\frac{\partial^2 C}{\partial y^2} - \frac{\partial S}{\partial t} \tag{5.14}$$

where,

$$\frac{\partial S}{\partial t} = \lambda C - \mu S \tag{5.15}$$

For the proposed problem the following initial and boundary conditions were considered:

- Initial condition:

$$S = C = 0, -a < y < a, \; t = 0 \tag{5.16}$$

- Boundary condition:

$$Ly_1 \frac{\partial C}{\partial t} = -D\frac{\partial C}{\partial y} \quad y = \text{-}\, a, t > 0 \tag{5.17}$$

$$Ly_2 \frac{\partial C}{\partial t} = -D\frac{\partial C}{\partial y} \quad y = +a, \; t > 0 \tag{5.18}$$

where Ly_1 and Ly_2 represent the distance between the solid surface and the bottom and top of the water tank, respectively. According to Eqs. (5.17) and (5.18), it is assumed that the rate of solute that leaves the solution is equal to the diffusive flux of solute at the surface of the plane sheet (see Fig. 5.3).

5.2.4.3 Solution Techniques: 1D Approach

Analytical Solution

Based on the works of Carter and Kibler [5] and Crank [10], Santos et al. [3] present the exact solution for the Eqs. (5.14) and (5.15) using the method of Laplace Transform. The application of the Laplace Transform consists in converting a partial differential equation in an ordinary differential equation which can be solved more easily. After this procedure, the inverse Laplace transform is calculated to get the original function of the problem that represent the solution of the governing equations [11, 12].

In order to obtain the exact solution of the physical problem, the model was simplified considering a porous plate with thickness $2R_2 = 2a$, immersed in a fluid (water) of height $(2L + 2a)$, where $Ly_2 = Ly_1 = L$ (Fig. 5.3).

The final equation for the concentration of free solute inside the solid during the water absorption process is obtained by considering the boundary conditions, the domain of the functions and with the use of necessary simplifications. This equation can be written as:

$$C(y,t) = \frac{LC_e}{L + (R+1)a} + \sum_{n=1}^{\infty} \frac{C_e \cos(k_n y) \mathrm{Exp}(p_n t)}{\cos(k_n a)\left\{1 + \left[1 + \frac{\mu\lambda}{(p_n+\mu)^2}\right]\left[\frac{Lp_n^2 a}{2D^2 k_n^2} + \frac{p_n}{2Dk_n^2} + \frac{a}{2L}\right]\right\}} \tag{5.19}$$

where p_n and k_n are eigenvalues and C_0 represent the initial solute concentration.

The final equation for the concentration of solute entrapped on the solid is written as:

$$S(y,t) = \left(\frac{\lambda}{\mu}\right)\frac{LC_e}{L + (R+1)a} + \sum_{n=1}^{\infty}\left(\frac{\lambda}{p_n + \mu}\right) \frac{C_e \cos(k_n y) \mathrm{Exp}(p_n t)}{\cos(k_n a)\left\{1 + \left[1 + \frac{\mu\lambda}{(p_n+\mu)^2}\right]\left[\frac{Lp_n^2 a}{2D^2 k_n^2} + \frac{p_n}{2Dk_n^2} + \frac{a}{2L}\right]\right\}} \tag{5.20}$$

The total moisture content inside the material in a specific position x and instant t is obtained from the sum of the amount of free solute and the amount of solute entrapped according with the following equation:

$$M = S + C \tag{5.21}$$

Based on Eq. (5.21), the average moisture content of the solid at different moments of the water uptake can be computed as follows:

$$\overline{M} = \frac{1}{V}\int_V M dV \tag{5.22}$$

or yet,

$$\overline{M} = \frac{1}{2a}\int_{-a}^{a} M(y,t) dy \tag{5.23}$$

where V is the volume of the solid.

From Eq. (5.23), the average moisture content of the solid at different water uptake times can be computed as follows:

$$\frac{\overline{M}}{M_e} = 1 - \sum_{n=1}^{\infty} \frac{(1+\alpha)e^{p_n t}}{1 + \left[1 + \frac{\mu\lambda}{(p_n+\mu)^2}\right]\left[\frac{Lp_n^2 a}{2D^2 k_n^2} + \frac{p_n}{2k_n^2 D} + \frac{a}{2L}\right]} \tag{5.24}$$

where:

$$\alpha = \frac{L}{(R+1)a} \tag{5.25}$$

$$M_e = \frac{LC_e}{(1+\alpha)a} \tag{5.26}$$

In Eq. (5.24), $\overline{M}$ corresponds to the total amount of solute, both free and immobilized to diffusion at a given time t, M_e corresponds to the amount of moisture at equilibrium, obtained after an infinite time, and $R = {}^{\lambda}/_{\mu}$. The terms p_n and k_n together form pairs of eigenvalues and aim to refine the approximate calculation and the results. Thus, the higher the number of eigenvalues, the more accurate the analytical results obtained. They correspond to non-zero roots of the Eq. (5.27) that are originated from applying Eqs. (5.19) in (5.18).

$$\frac{Lp}{D} = k \tan(k \times a) \tag{5.27}$$

In Eq. (5.27), the values of k are given by:

$$k^2 = -\frac{p}{D}\left(\frac{p+\mu+\lambda}{p+\mu}\right) \tag{5.28}$$

For a 3D physical situation, the analytical solution can be obtained as the product of the analytical solution for three infinite plates. In this case, each of the plates must have thickness equal to $2R_1$, $2R_2$ and $2R_3$. Special care must be given in the determination of the eigenvalues p and k, which are different for each of the x, y and z diretions [2, 13–15].

Numerical Solution

The numerical solution of a partial differential equation basically consists of two steps: (a) discretizing the physical domain under study in several sub domains and (b) transforming the governing equation into a linear algebraic equation in the discretized form applied to each sub domain contained in the solid under investigation. After these procedures, the result is a set of linear algebraic equations whose solution provides the distribution of the potential unknown inside the domain and in time.

Herein, the finite-volume method for numerical solution of the governing equation [16–18] was used. For the discretization of Eqs. (5.14) and (5.15), the continuous solid of a thickness 2a was subdivided in (np-2) control volumes, as shown in Fig. 5.4.

In Fig. 5.4 each control volume has thickness Δx; S, P and N represent nodal points, while s and n represent the left and right faces of the control volume P,

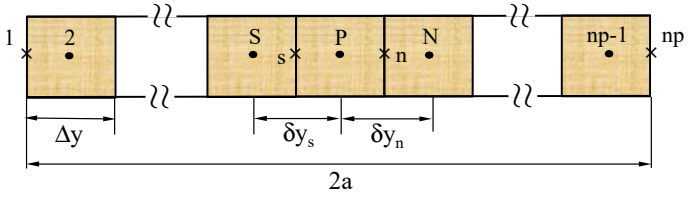

Fig. 5.4 Representation of the one-dimensional simulation domain with (np-2) control volumes

respectively; δy_s and δy_n represent the distance between nodal point P and nodal points S and N, respectively.

(a) **Solution for the concentration of free solute**

- ***Internal points***

In the finite volume method, discretization is done by integrating all terms of Eq. (5.14) in volume and time. Thus, after integration and using a fully implicit formulation, rearranging the terms in the linearized discrete algebraic form at P, leads to:

$$A_P C_P = A_N C_N + A_S C_S + A_P^o C_P^o + B_P^C \tag{5.29}$$

where,

$$A_P = \left(\frac{\Delta x}{\Delta t} + \frac{D_n}{\delta x_n} + \frac{D_s}{\delta x_s} + \lambda \Delta x \right) \tag{5.30}$$

$$A_N = \frac{D_n}{\delta y_n} \tag{5.31}$$

$$A_S = \frac{D_s}{\delta y_s} \tag{5.32}$$

$$A_P^o = \frac{\Delta y}{\Delta t} \tag{5.33}$$

$$B_P^C = \mu \Delta y S_P^o \tag{5.34}$$

where the coefficients A_P, A_N, and A_S are the conductance between the nodal points P and their corresponding neighbors. The term A_P^o represents the influence of the value of C on the value of C at t prior to that at the current time t. Equation (5.29) is valid for all internal points of the domain except for the boundary and symmetry points.

- ***Bottom boundary points***

In this case, the boundary flux is replaced by the existing boundary condition (Eq. 5.17). By doing this, the linear discretized equation for the bottom boundary points is:

$$A_P C_P = A_N C_N + A_s^o C_s^o + A_P^o C_P^o + B_P^C \tag{5.35}$$

where,

$$A_P = \frac{\Delta y}{\Delta t} + \frac{D_n}{\delta\, y_n} + \frac{1}{\left(\frac{\delta y_s}{D_s} + \frac{\Delta t}{Ly_1}\right)} \tag{5.36}$$

$$A_N = \frac{D_n}{\delta y_n} \tag{5.37}$$

$$A_s^o = \frac{1}{\left(\frac{\delta y_s}{D_s} + \frac{\Delta t}{Ly_1}\right)} \tag{5.38}$$

$$A_P^o = \frac{\Delta y}{\Delta t} \tag{5.39}$$

$$B_P^C = \mu \Delta y S_P^o \tag{5.40}$$

- ***Upper boundary points***

In this case, the boundary flux that must be replaced by the existing boundary condition (Eq. 5.18) and the linear discretized equation for the boundary points is given by:

$$A_P C_P = A_S C_S + A_n^o C_n^o + A_P^o C_P^o + B_P^C \tag{5.41}$$

where,

$$A_P = \frac{\Delta y}{\Delta t} + \frac{D_s}{\delta\, y_s} + \frac{1}{\left(\frac{\delta y_n}{D_n} + \frac{\Delta t}{Ly_2}\right)} \tag{5.42}$$

$$A_S = \frac{D_s}{\delta y_s} \tag{5.43}$$

$$A_n^o = \frac{1}{\left(\frac{\delta y_n}{D_n} + \frac{\Delta t}{Ly_2}\right)} \tag{5.44}$$

$$A_P^o = \frac{\Delta y}{\Delta t} \tag{5.45}$$

$$B_P^C = \mu \Delta y S_P^o \tag{5.46}$$

Equations 5.29, 5.35 and 5.41 when applied at each of the control volumes form a system of algebraic linear equations whose solution indicates the concentration of free solute within the solid during the water absorption process.

(b) **Solution for the concentration of entrapped solute**

In order to obtain the equations associated to the concentration of entrapped solute in the solid, Eq. (5.15) is integrated in volume and time. Reorganizing the terms, we obtain the following linear algebraic equation, valid for all control volume of the domain:

$$A_P S_P = A_P^o S_P^o + B_P^S \tag{5.47}$$

where,

$$A_P = \frac{\Delta y}{\Delta t} + \mu \Delta y \tag{5.48}$$

$$A_P^o = \frac{\Delta y}{\Delta t} \tag{5.49}$$

$$B_P^S = \lambda \Delta y C_P \tag{5.50}$$

It is important to notice that the Eq. (5.47) is an explicit equation, depending only of the values of the free solute concentration at each nodal point and time.

The total moisture inside the material in a specific position x and instant t is given by summing the amounts of free and entrapped solute as follows:

$$M = S + C \tag{5.51}$$

Equation (5.23) yields the average moisture content of the solid at any time. This equation in the discretized form is written as:

$$\overline{M} = \frac{1}{2a} \sum_{i=2}^{np-1} M_i \Delta y_i \tag{5.52}$$

where np represents the total number of nodal points considered.

The linear algebraic equation system can be solved iteratively using the Gauss–Seidel method, where is assumed that the numerical solution converges when, from the initial condition, the following criterion is satisfied at each nodal point of the domain, at a given time:

$$\left|C_P^{n+1} - C_P^n\right| \leq 10^{-10} \tag{5.53}$$

where n represents the nth iteration at each instant. To obtain the predicted results, a time step and mesh refinement study was performed. After this process a grid with np = 20 nodal points and a time step $\Delta t = 20$ s was chosen.

(c) **Estimation of the model parameters**

For the computer simulation of the water absorption process using the Langmuir-type modl, it is necessary to use D, λ and μ values consistent with the experimental data. This procedure is described in detail below.

- ***Initial estimate of the probabilities λ and μ***

Considering a one-dimensional approach, $\kappa = \pi^2 D/(2R_2)^2$ and satisfying $2\lambda << \kappa$ and $2\mu << \kappa$, the following approximate solution for determining the average moisture content (Eq. 5.24) is valid [5]:

$$\frac{\overline{M}}{M_e} = \frac{\mu}{\lambda+\mu} e^{-\lambda t}\left[1 - \frac{8}{\pi^2}\sum_{n=1}^{\infty}\frac{e^{-\kappa(2n+1)^2 t}}{(2n+1)^2}\right] + \frac{\mu}{\lambda+\mu}\left(e^{-\mu t} - e^{-\lambda t}\right) + \left(1 - e^{-\mu t}\right) \tag{5.54}$$

For long times, when $\kappa \times t >> 1$, Eq. (5.54) is reduced to:

$$\frac{\overline{M}}{M_e} = 1 - \frac{\lambda}{\lambda+\mu}\mathrm{Exp}(-\mu \times t) \tag{5.55}$$

which can be written, as follows:

$$\frac{\overline{M}}{M_e} = 1 - A\mathrm{Exp}(-B \times t) \tag{5.56}$$

where

$$A = \frac{\lambda}{\lambda+\mu} \tag{5.57}$$

$$B = \mu \tag{5.58}$$

With the values of the average moisture content over time obtained experimentally, it is possible to perform a nonlinear regression of Eq. (5.56), to obtain the values of A and B statistical parameters and, with those, determine the values of λ and μ parameters using Eqs. (5.57) and (5.58).

- ***Initial estimate of the probabilities λ and μ***

In this case, considering a one-dimensional approach, for short times ($t \leq 0.7/\kappa$), the following approximate solution for determining the average moisture content (Eq. 5.59) is valid [5]:

$$\overline{\mathrm{M}} = \frac{4}{\pi^{3/2}}\left(\frac{\mu}{\lambda+\mu}\mathrm{M_e}\right)\sqrt{\kappa \times \mathrm{t}} \tag{5.59}$$

or yet,

$$\overline{\mathrm{M}} = \frac{4}{\pi^{3/2}}\left(\frac{\mu}{\lambda+\mu}\mathrm{M_e}\right)\sqrt{\kappa} \times \sqrt{\mathrm{t}} \tag{5.60}$$

Thus, substituting $\kappa = \pi^2 D/(2R_2)^2$ in Eq. (5.60) we get:

$$\overline{M} = \frac{4}{\pi^{3/2}}\left(\frac{\mu}{\lambda+\mu}M_e\right)\sqrt{\frac{\pi^2 D}{(2R_2)^2}} \times \sqrt{t} \tag{5.61}$$

Calculating the derivative of Eq. (5.61) with respect to time and since, for initial times, the behavior of the average moisture content is approximately linear with time, we can write:

$$\frac{d\overline{M}}{d\sqrt{t}} \approx \frac{\overline{M}_2 - \overline{M}_1}{\sqrt{t_2} - \sqrt{t_1}} = \left(\frac{4}{\pi^{3/2}}\right)\left(\frac{\mu}{\lambda+\mu}M_e\right)\left(\frac{\pi}{2R_2}\right) \times \sqrt{D} \tag{5.62}$$

which leads to:

$$D = \pi \times \left(\frac{R_2}{2M_e}\right)^2 \left(\frac{\lambda+\mu}{\mu}\right)^2 \left(\frac{\overline{M}_2 - \overline{M}_1}{\sqrt{t_2} - \sqrt{t_1}}\right)^2 \tag{5.63}$$

where $\overline{M}_1$ and $\overline{M}_2$ are values of the average moisture content obtained experimentally, at times t_1 and t_2, respectively, and M_e is the equilibrium moisture content.

An alternative method to estimate the mass diffusion coefficient is to consider $\lambda = 0$ (Langmuir-type model tending to the Fick´s model) and determine D using the least square error technique to minimize the error between theoretical and experimental data (Eq. 5.64).

It is important to notice that the model parameters D, μ, and λ determined as already mentioned are only an initial estimate and that the mathematical procedures reported above can also be used for a three-dimensional analysis.

Table 5.1 Geometrical parameters used in the simulation

Parameter	Value
L (m)	0.3
a (m)	1.5×10^{-3}

- ***Actual estimate of the parameters D, μ, and λ***

Once the initial estimate of parameters D, μ and λ was made, the real estimate of these parameters can be performed, comparing the least square error between the predicted and experimental data of the average moisture content, and varying these parameters until a minimum error is reached, according to Eq. (5.64).

$$ERQM = \sum_{i=1}^{n} \left[\overline{M}_{predict} - \overline{M}_{experimental}\right]^2 \tag{5.64}$$

where n is the number of experimental points.

5.2.4.4 Langmuir-Type Model Application: 1D Approach

Analytical and Numerical Results

- ***Absorbed Water Kinetics***

The exact and numerical solutions of the governing equations were applied to predict moisture diffusion in polymer composites reinforced with caroá fibers. As already mentioned, the composites studied have width and length greater that its thickness. The results that presented here refer to the case where $Ly_2 = Ly_1 = L$ and $R_2 = a$. It is assumed that water penetrates only in the thickness. direction. Table 5.1 presents the geometric parameters used in the simulation.

For the validation of the model, the predicted result of the average moisture content was compared with analytical results reported by Santos et al. [3] and the experimental data reported by Silva [19] and Nóbrega et al. [20] for polymer composite materials reinforced with Caroá fiber (T = 25 °C). From this comparison, the mass diffusion coefficient and the probabilities μ and λ, of the model were estimated using the least squares error technique, given by the following equation:

$$ERQM = \sum_{i=1}^{n} \left[\overline{M}_{predicted} - \overline{M}_{experimental}\right]^2 \tag{5.54}$$

where n is the number of experimental points. According to Santos et al. [3], an average quadratic error of 0.047467 $kg_{water}/kg_{dry\ solid}$) was obtained. Table 5.2 shows the estimated data.

Table 5.2 Physical parameters used in the simulation

Parameter	Value
D (m^2s^{-1})	7.020×10^{-12}
μ (s^{-1})	1.697×10^{-6}
λ (s^{-1})	0.836×10^{-6}

Table 5.3 Some values of the p and k eigenvalues

n	k_n (m^{-1})	P_n (m^{-1})
1	1049.07	-7.5768×10^{-6}
2	1058.21	-1.29658×10^{-6}
3	3142.29	-6.06761×10^{-6}
4	3171.09	-1.44941×10^{-6}
5	5236.41	-1.67169×10^{-6}

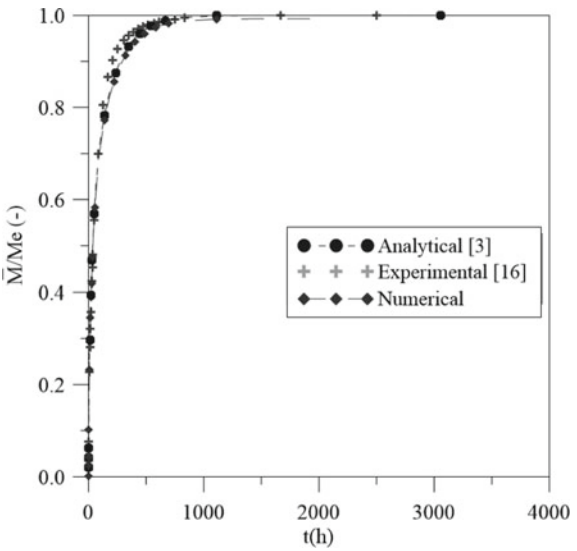

Fig. 5.5 Numerical, analytical and experimental dimensionless average moisture content of polymer composites reinforced with caroá fiber during the water absorption process (T = 25 °C, $Ly_2 = Ly_1 = 0.3$ m)

These values led to 30 pairs of eigenvalues and one pair of imaginary root which were used to obtain the exact solution of Eqs. (5.19), (5.20) and (5.24). Table 5.3 presents five values of p_n and k_n engeinvalues determined by Santos et al. [3].

Figure 5.5 illustrates the comparison between numerical, analytical and experimental data of the average moisture content obtained during water absorption in caroá fiber-reinforced polymer composites immersed in water at 25 °C.

Figure 5.5 shows some discrepancies between experimental and numerical data, which can be attributed to the lack of suitable boundary conditions for the model and the assumption of constant properties. The numerical results, however, showed good

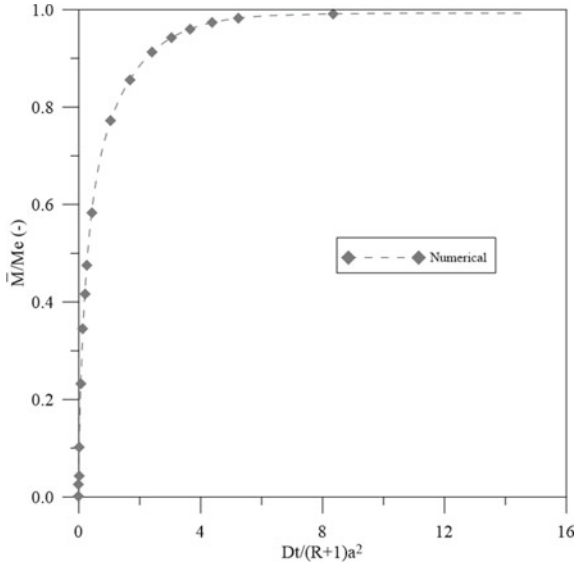

Fig. 5.6 Dimensionless average moisture content of the caroá fiber reinforced polymer composite as a function of modified Fourier number of mass transfer during the water absorption process (T = 25 °C, Ly_2 = Ly_1 = 0.3 m)

agreement with analytical results, indicating that the proposed mathematical model properly describes the water diffusion process inside the material.

A more general mathematical analysis was obtained by plotting the dimesionless average moisture content as a function of another dimensioless parameter Fo = Dt/[(R + 1)a^2] namely modified Fourier number for mass transfer. These results are shown in Fig. 5.6.This procedure allows for results to be independent of mass diffusivity, λ and μ probabilities, composite thickness and time. Analysis of this figure indicates that water sorption is very quick in the early stages up to a modified Fourier number of mass transfer of approximately 2.0, and tends to decline for long exposure times until equilibrium is achieved (saturation condition, $M_e = 14.488\%$), where the dimensionless average moisture content tends to a maximum value. The time to achieve the hygroscopic equilibrium was estimated to Fo $\cong 10F_o \approx 12$.

- ***Absorbed Free and Entrapped Water Molecules Distribution***

Figure 5.7 shows the variation of dimensionless free solute concentration (analytical and numerical) along the thickness of the solid, given by C/Ce, where Ce (estimated by Eq. 5.22 as Ce = 0.09778 kg/kg) represents the equilibrium concentration of the solute in the fluid medium. Since the solid in question is symmetrical with respect to its center, results are ploted only from the center (y = 0 m) to the composite surface (y = 0.0015 m). This figure shows that, for shorter times, moisture concentration variation is higher close to the surface of the material, that is, there is a high concentration gradient of free water, in these regions. With increasing time, this relationship tends to approach 1.0, as the hygroscopic equilibrium condition (saturation) is reached. Besides, at any point within the solid, the moisture content increases with time until it reaches equilibrium.

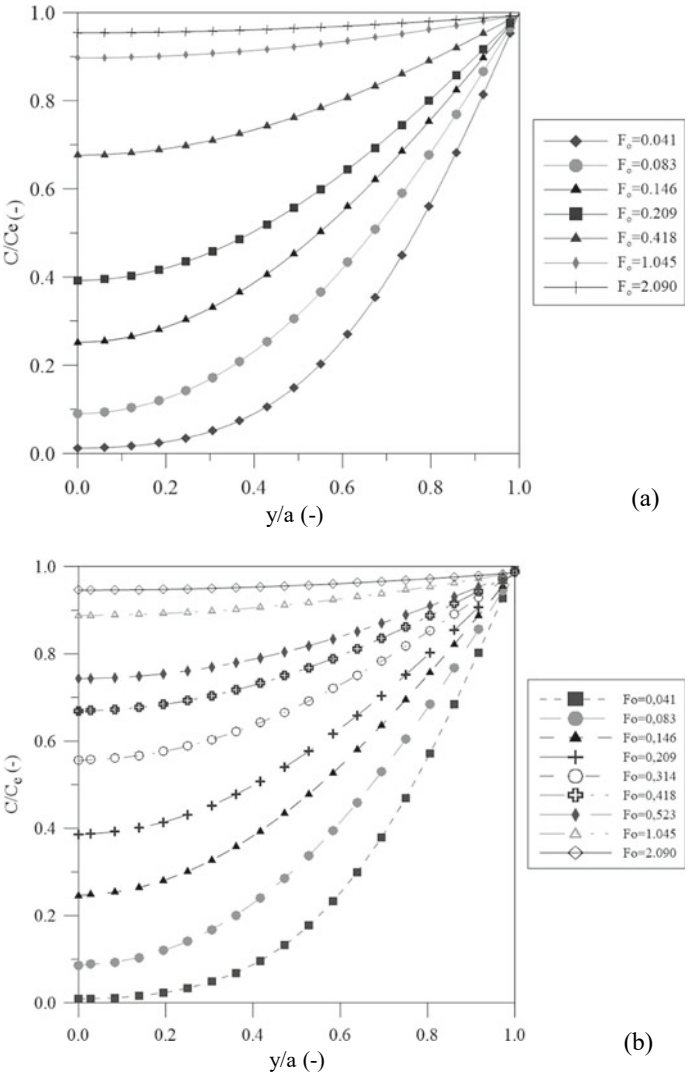

Fig. 5.7 Dimensionless free solute concentration distribution inside the caroá fiber reinforced plymer composite for different modified Fourier number of mass transfer. **a** Analytical and **b** Numerical results (T = 25 °C, Ly2 = Ly1 = 0.3 m)

Figure 5.8 illustrates the distribution of the dimensionless bound (entrapped) water molecules (numerical) along the thickness of the caroá fiber-reinforced polymer composite. Analysis of this figure shows that an increase in the content of bound water molecules depends on the increase in the concentration of free water molecules into the material. The major bound water concentration gradients are found near the solid surface. For longer times, or when there is a greater amount of free water molecules

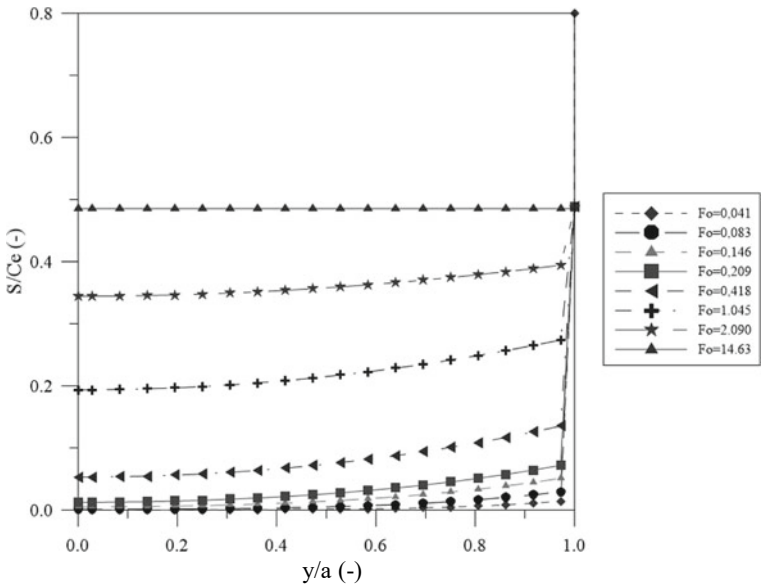

Fig. 5.8 Predicted dimensionless entrapped solute concentration inside the caroá fiber reinforced plymer composite for different modified Fourier number of mass transfer (T = 25 °C, Ly2 = Ly1 = 0.3 m)

within the material, there is a higher number of entrapped water molecules, and this condition occurs until that equilibrium is reached. This occurs as $\partial S/\partial t = 0$, or yet, $\lambda C = \mu S$, which implies that $S/C_e = \lambda/\mu = 0.493$, for $t \to \infty$.

At the beginning, the observed behaviour for water absorption is Fickian, that is, there is moisture migration of water molecules in "free" state. However, as time goes by and as more moisture is absorbed, the water diffusion rate decreases. This behaviour is explained by two phenomena: (a) as water absorbed more molecules are linked to the polymer chains, thus reducing the amount of water that can be absorbed, and (b) the relaxation rate becomes larger than the diffusion rate, controlling the final stages of the process.

Figure 5.9 shows the dimensionless moisture content absorbed into the material, obtained by the sum of the free water molecules concentration and the entrapped water molecules concentration. In regions near the surface, water absorption is faster, because there is a larger area in direct contact with water bath. The water penetrates the interior of the material generating a higher moisture content gradient along the thickness, which decreases with increasing immersion time. Thus, at any point inside the solid, the moisture content increases with time until it reaches equilibrium, i.e., its saturation point. It is intuitive to say that at longer immersion times there is an increase in the amount of molecules entrapped within the material while the amount of free molecules to diffuse decreases.

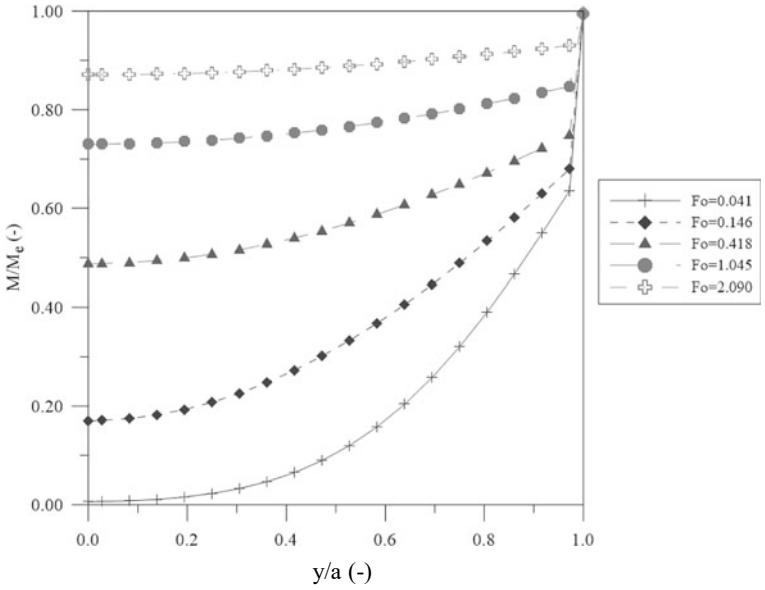

Fig. 5.9 Predicted dimensionless misture content inside the caroá fiber reinforced plymer composite for different modified Fourier number of mass transfer (T = 25 °C, $Ly_2 = Ly_1 = 0.3$ m)

For a more complex physical situation, for example, where $Ly_2 \neq Ly_1$, Melo et al. [21] reported a theoretical analysis aiming to evaluate the effect of the water layer thickness (upper and bottom) on the water absorption behavior inside the material. In that research, the authors considered equilibrium moisture content Me = 0.14488 kg/kg, water bath temperature 25 °C, and total process time 2250 h. Table 1 summarizes the data used in the simulations.

Figure 5.10 illustrates the average moisture content in the material along the process for different arbitrary cases, as reported in Table 5.4. Figure 5.11 shows the local moisture contents obtained from the sum of the free and bound water molecule concentrations along the thickness of the material for different elapsed times and distances from the composite surface to maximum water level in the container. Figure 5.12 shows the behavior of the variation rate of the local moisture content as a function of time in the center of the composite.

According to Melo et al. [21], water absorption kinetics is strongly affected by the water layer thickness, the moisture content gradient, and the equilibrium moisture content inside the material. These authors verified that the higher gradients are found in the regions where Ly_1 or Ly_2 have higher value. Furthermore, the largest concentration gradients of free and entrapped water molecules are at the composite surface, and an asymmetric behavior of the process variables is obtained when the geometric parameters Ly_2 and Ly_1 are different.

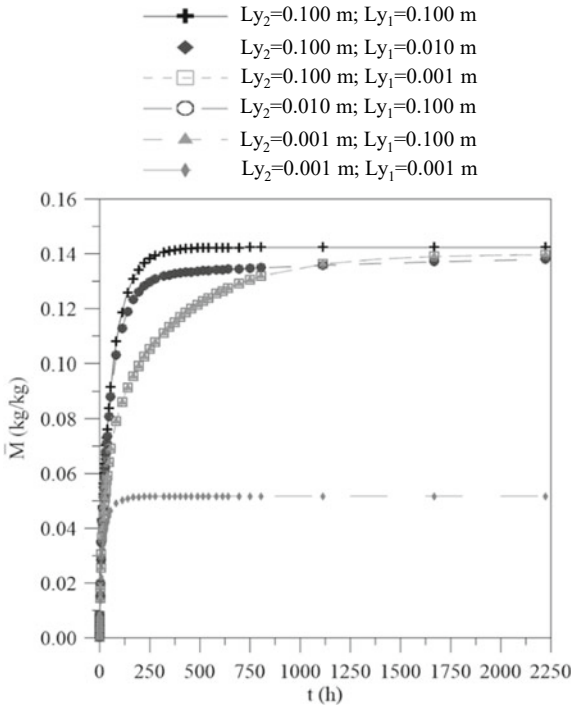

Fig. 5.10 **a** Average moisture content as a function of the process time for different physical saturations. **b** Detailed view of **a**

Table 5.4 Process parameters values of the polymer composite used in the simulations

To (°C)	2a (m)	Ly_2 (m)	Ly_1 (m)	μ (10^{-6} s^{-1})	λ (10^{-6} s^{-1})	D (10^{-12} m^2s^{-1})
25	0.003	0.100	0.100	5	1	5
25	0.003	0.100	0.010	5	1	5
25	0.003	0.100	0.001	5	1	5
25	0.003	0.010	0.100	5	1	5
25	0.003	0.001	0.100	5	1	5
25	0.003	0.001	0.001	5	1	5

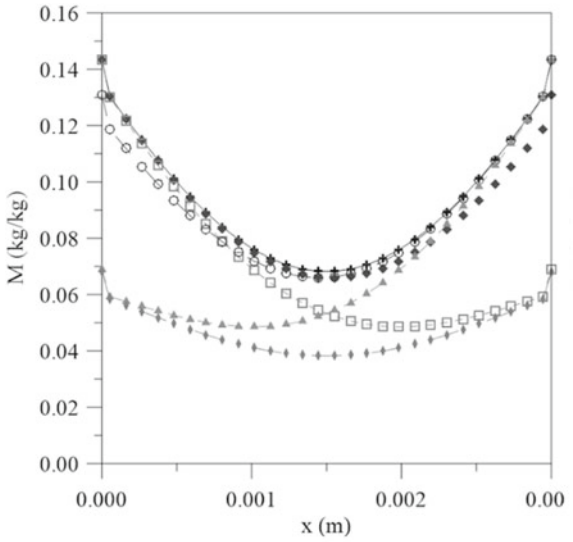

(a) 56 h

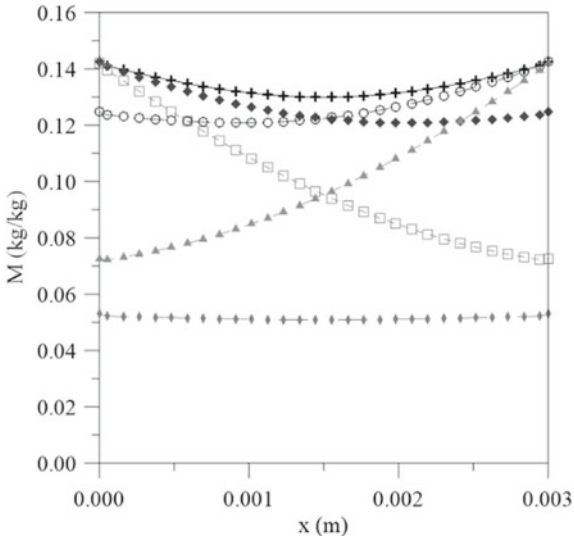

(b) 195 h

Fig. 5.11 Local moisture content as function of the position inside the material at different process times

5.2.5 The Water Absorption Process: 3D Approach

5.2.5.1 Solution Techniques: 3D Approach

Numerical Solution

The finite volume method was used for the three-dimensional numerical solution of the governing equations applied to moisture absorption in polymer composites

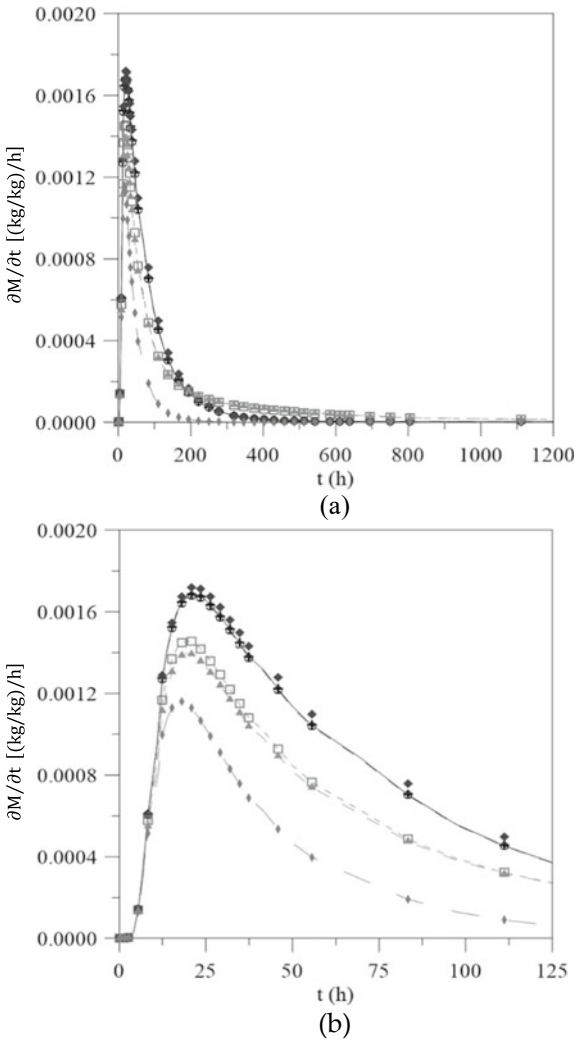

Fig. 5.12 Temporal variation rate of the local moisture content in the center of the polymer composite **a** and detail of the figure **b**

with parallelepipedic form, as reported by Santos et al. [22, 23], Brito et al. [24] and Santos [25]. In this solution, a fully implicit formulation for the concentration of free solute and explicit formulation for the concentration of trapped solute were used. Figure 5.13 illustrates a control volume (sub domain) used for discretization of the governing equations. The nodal point P (in the center of the control volume), its adjacent neighbors W, E, S, N, T, and F, the distances between these nodal points, and the dimensions Δx, Δy, and Δz, of the control volume are also shown in this Figure.

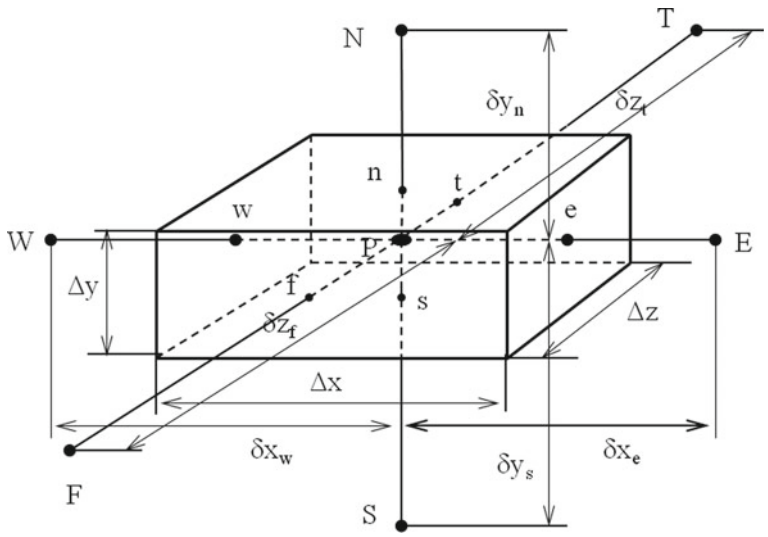

Fig. 5.13 Three-dimensional control volume used in this work

Complete detailing of the numerical procedure used for the solution of the governing equations is given below.

(a) **Solution for the Free Water Molecules Concentration**

- ***Internal points***

The numerical solution of Eq. (5.3) is obtained by integrating it in volume and time. Assuming a fully implicit formulation, one can write the Eq. (5.3) in its discretized linear form as follows:

$$A_P C_P = A_E C_E + A_W C_W + A_N C_N + A_S C_S + A_F C_F + A_T C_T$$

$$+ A_P^o C_P^o + B_P^C \tag{5.66}$$

where:

$$A_E = \frac{D_e}{\delta x_e} \Delta y \Delta z \tag{5.67}$$

$$A_W = \frac{D_w}{\delta x_w} \Delta y \Delta z \tag{5.68}$$

$$A_N = \frac{D_n}{\delta y_n} \Delta x \Delta z \tag{5.69}$$

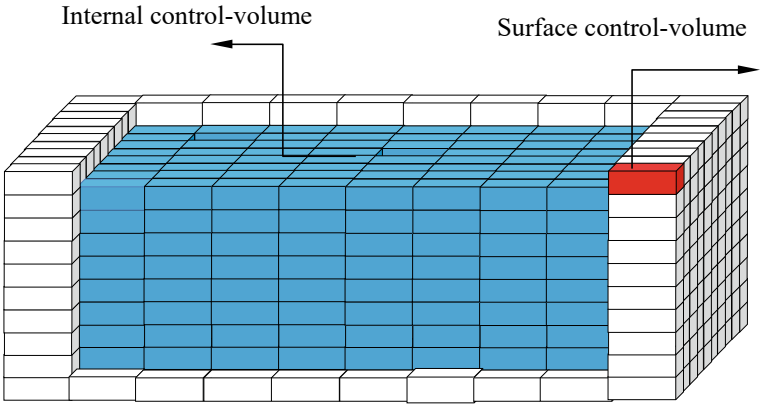

Fig. 5.14 Numerical grid showing the internal and surface control-volumes

$$A_S = \frac{D_s}{\delta y_s}\Delta x \Delta z \tag{5.70}$$

$$A_F = \frac{D_f}{\delta z_f}\Delta y \Delta x \tag{5.71}$$

$$A_T = \frac{D_t}{\delta z_t}\Delta y \Delta x \tag{5.72}$$

$$A_P^o = \frac{\Delta x \Delta y \Delta z}{\Delta t} \tag{5.73}$$

$$A_P = \frac{\Delta x \Delta y \Delta z}{\Delta t} + \frac{D_e}{\delta x_e}\Delta y \Delta z + \frac{D_w}{\delta x_w}\Delta y \Delta z + \frac{D_n}{\delta y_n}\Delta x \Delta z + \frac{D_s}{\delta y_s}\Delta x \Delta z$$

$$+ \frac{D_f}{\delta z_f}\Delta y \Delta x + \frac{D_t}{\delta z_t}\Delta y \Delta x \tag{5.74}$$

$$B_P^C = -\left(S_P - S_P^o\right)\frac{\Delta x \Delta y \Delta z}{\Delta t} \tag{5.75}$$

- ***Boundary points***

It should be noted that Eq. (5.66) is only applied to the internal control volumes of the computational domain (Fig. 5.14). For the other control volumes (symmetry and border), a mass balance in each one of them is performed. In total, there are 27 different types of control volumes. As an example, the result of Eq. 5.3 applied to the control volume of the right upper corner of the computational domain, as shown in Fig. 5.14, is given by the following equation:

$$A_P C_P = A_W C_W + A_S C_S + A_T C_T + A_P^o C_P^o + B_P^C \tag{5.76}$$

where:

$$A_W = \frac{D_w^C}{\delta x_w} \Delta y \Delta z \tag{5.77}$$

$$A_S = \frac{D_s}{\delta y_s} \Delta x \Delta z \tag{5.78}$$

$$A_T = \frac{D_t}{\delta z_t} \Delta y \Delta x \tag{5.79}$$

$$A_P^o = \frac{\Delta x \Delta y \Delta z}{\Delta t} \tag{5.80}$$

$$A_P = \frac{\Delta \mathrm{x} \Delta \mathrm{y} \Delta \mathrm{z}}{\Delta \mathrm{t}} + \frac{\mathrm{D_w}}{\delta \mathrm{x_w}} \Delta \mathrm{y} \Delta \mathrm{z} + \frac{\mathrm{D_s}}{\delta \mathrm{y_s}} \Delta \mathrm{x} \Delta \mathrm{z} + \frac{\mathrm{D_t}}{\delta \mathrm{z_t}} \Delta \mathrm{y} \Delta \mathrm{x} + \frac{\Delta \mathrm{y} \Delta \mathrm{x}}{\left(\frac{\delta \mathrm{z_f}}{\mathrm{D_f}} + \frac{\Delta \mathrm{t}}{l_z} \right)} + \frac{\Delta \mathrm{z} \Delta \mathrm{x}}{\left(\frac{\delta \mathrm{y_n}}{\mathrm{D_n}} + \frac{\Delta \mathrm{t}}{l_y} \right)} + \frac{\Delta \mathrm{y} \Delta \mathrm{z}}{\left(\frac{\delta \mathrm{x_e}}{\mathrm{D_e}} + \frac{\Delta \mathrm{t}}{l_x} \right)} \tag{5.81}$$

$$\mathrm{B_P^C} = \frac{\mathrm{C_f^o} \Delta \mathrm{x} \Delta \mathrm{y}}{\left(\frac{\delta \mathrm{z_f}}{\mathrm{D_f}} + \frac{\Delta \mathrm{t}}{l_z} \right)} + \frac{\mathrm{C_e^o} \Delta \mathrm{y} \Delta \mathrm{z}}{\left(\frac{\delta \mathrm{x_e}}{\mathrm{D_e}} + \frac{\Delta \mathrm{t}}{l_x} \right)} + \frac{\mathrm{C_n^o} \Delta \mathrm{x} \Delta \mathrm{z}}{\left(\frac{\delta \mathrm{y_n}}{\mathrm{D_n}} + \frac{\Delta \mathrm{t}}{l_y} \right)} - \left(\mathrm{S_P} - \mathrm{S_P^o} \right) \frac{\Delta \mathrm{x} \Delta \mathrm{y} \Delta \mathrm{z}}{\Delta \mathrm{t}} \tag{5.82}$$

(b) **Solution for the entrapped water molecules concentration**

The numerical solution of Eq. (5.4) is obtained by integrating it in volume and time. Assuming an explicit formulation, one can write the Eq. 5.4, in its discretized linear form, as follows:

$$A_P S_P = A_P^o S_P^o + B_P^S \tag{5.83}$$

where:

$$A_P^o = \frac{\Delta x \Delta y \Delta z}{\Delta t} \tag{5.84}$$

$$A_P = \frac{\Delta x \Delta y \Delta z}{\Delta t} + \mu \Delta x \Delta y \Delta z \tag{5.85}$$

$$B_P^S = \lambda C_P \Delta x \Delta y \Delta z \tag{5.86}$$

In the discretized form, the local and average moisture contents can be written, respectively, as follows:

$$M_{i,j,k} = C_{i,j,k} + S_{i,j,k} \tag{5.87}$$

$$\overline{M} = \frac{1}{V} \sum_{i=2}^{npx-1} \sum_{j=2}^{npy-1} \sum_{k=2}^{npz-1} M_{i,j,k} \Delta V_{i,j,k} \tag{5.88}$$

in which i, j e k represent the position of the nodal point in the x, y, and z directions, respectively, and npx, npy and npz are the nodal point numbers in the x, y, and z directions respectively.

From the discretization of the governing equations, a system of liear algebraic equations is generated that must be solved to obtain the values of C, S and M within the material throughout the process. The Gauss–Seidel iterative method can be used for solving this system of algebraic equations. In order to obtain the numerical results, simulations were performed using a grid with $20 \times 20 \times 20$ nodal points and time step $\Delta t = 20$ s. Other details about this numerical procedure can found in the references already cited in this chapter.

5.2.5.2 Langmuir-Type Model Application: Three-Dimensional Approach

Numerical Results

Based on the references already mentioned, the influence of the geometrical parameter L_y (see Fig. 5.2), in the process of water absorption in fiber-reinforced polymer composites was evaluated. For this analysis, the authors considered $\mu = \lambda = 1.0 \times 10^{-6}$ s^{-1}, $D = 1 \times 10^{-12}$ m^2/s, $R_1 = R_3 = 0.0100$ m, $R_2 = 0.0015$ m, $R_3 = 0.000$ m, $Lx_1 = Lx_2 = 0.1000$ m, $Lz_1 = Lz_2 = 0.1000$ m and $Ly_1 = Ly_2 = 0.0010$ m, 0.0100 m and 01,000 m,

The obtained results indicated that variations in L_y values strongly affect the average moisture content, and also average free and entrapped water molecules concentrations. The higher the L_y value, the higher the water layer close to the composite wall and the faster the water absorption rate. For initial times of the process, the differences among the predicted results are not significant, however, in the course of the process a different behavior of the water absorption kinetics can be clearly observed.

Upon analyzing the free water molecules concentration distribution was verified that, for small value of L_y, there is essentially no free water flux in the y-direction but, in the opposite directions, the water flux is more intense and free water molecules move horizontally (x—and z—directions) with nearly equal velocities.

A similar behavior for the distribution of entrapped water molecules concentration to that presented by free solute concentration was observed. In general, the geometric parameter L_y affects both the distribution of free and entrapped solute concentration and, as a result, the total moisture content of the composite immersed in water.

Besides, it was observed small values of the bound water molecules concentration when compared to unbound water molecules concentration. Furthermore, a transient analysis of the predicted results showed that the free water molecules concentration is increasing from the composite surface to its center with a horizontal flux of moisture. Compared with the y-direction, the greatest moisture fluxes occur in x and z- direction. The same behavior is observed when the entrapped water molecules concentration is considered. Nevertheless, entrapped water concentration increases more slowly than free water molecules concentration, mainly at the initial process times.

As final comment, we notice that water absorption is facilitated when polymer molecules have clusters capable of forming hydrogen bonds. Plant fibers are rich in cellulose, hemicellulose and lignin which have hydroxyl groups, i.e., have high affinity for water. The absorption of water by the resin, in turn, can be considered practically null, since it has a considerable hydrophobic character [26]. Addition of the plant fibers to hydrophobic resins leads to an increase in the water absorption levels, so an important parameter to be analyzed is how much water is absorbed by the material over time.

The effects caused by long time exposure to moisture may be irreversible due to the water molecules affinity with specific functional groups of the polymeric matrices. Destructive changes usually occur due to degradation of existing physical–chemical interactions between the resin and fiber and, as a consequence, there are changes in the fiber, causing delamination and reduction in the composite material properties. Thus, understanding of the water absorption process is crucial to predict the quality of the material e wet environments.

From the physical and mathematical point of views is important to analyse quantitatively what happens with the general solution for the extreme values of the probability μ which correspond to very fast or very slow process. When μ is very large as compared to λ., the process is very rapid compared with diffusion. In this situation, the immobilized component is in equilibrium with the component free to diffuse into the composite, or yet, the number of free molecules that become entrapped and remain entrapped by a time long enough to hinder diffusion is very small, and process is controlled by diffusion. However, if $\mu \to 0$, the process is infinitely slow, the composite is occuped, by simple diffusion, and only a fraction of solute (moisture) can be accommodated in the freely diffusing state and none in the immobilized state. On the other hand, when λ increases sufficiently, moisture absorption is hindered due to the higher probability that a free water molecule will become entrapped instead of freely diffusing into the composite [10, 13]. Further, for the case where D is very large, the diffusion is so rapid that the concentration of free and immobilized solute (water) are almost uniform through the composite during the water uptake process.

From the explanation above it is possible to conclude that variations in the mass diffusion coefficient and the probabilities that water molecules are free or entrapped, deeply modifies the water absorption process, which proves the great potential of the Langmuir-type model and its ability of adequately describing moisture migration behaviour inside the polymer composite.

References

1. Bonniau, P., Bunsell, A.R.: A comparative study of water absorption theories applied to glass epoxy composites. J. Compos. Mater. **15**(3), 272–293 (1981)
2. Grace, L.R., Altan, M.C.: Characterization of anisotropic moisture absorption in polymeric composites using hindered diffusion model. Compos. A Appl. Sci. Manuf. **43**(8), 1187–1196 (2012)
3. Santos, W.R.G., Melo, R.Q.C., Lima, A.G.B.: Water absorption in polymer composites reinforced with vegetable fiber using Langmuir-type model: An exact mathematical treatment. Defect Diffus. For. **371**, 102–110 (2016)
4. Perreux, D., Suri, C.: A study of the coupling between the phenomena of water absorption and damage in glass/epoxy composite pipes. Compos. Sci. Technol. **57**(9–10), 1403–1413 (1997)
5. Carter, H.G., Kibler, K.G.: Langmuir-type model for anomalous moisture diffusion in composite resins. J. Compos. Mater. **12**(2), 118–131 (1978)
6. Glaskova, T.I., Guedes, R.M., Morais, J.J., Aniskevich, A.N.: A comparative analysis of moisture transport models as applied to an epoxy binder. Mech. Compos. Mater. **43**(4), 377–388 (2007)
7. Cotinaud, M., Bonniau, P., Bunsell, A.R.: The effect of water absorption on the electrical properties of glass-fibre reinforced epoxy composites. J. Mater. Sci. **17**(3), 867–877 (1982)
8. Apicella, A., Estiziano, L., Nicolais, L., Tucci, V.: Environmental degradation of the electrical and thermal properties of organic insulating materials. J. Mater. Sci. **23**(2), 729–735 (1988)
9. Popineau, S., Rondeau-Mouro, C., Sulpice-Gaillet, C., Shanahan, M.E.: Free/bound water absorption in an epoxy adhesive. Polymer **46**(24), 10733–10740 (2005)
10. Crank, J.: The mathematics of diffusion, 2nd edn. Oxford University Press, Oxford (1975)
11. Fu, Z., Chen, W., Yang, H.: Boundary particle method for laplace transformed time fractional diffusion equations. J. Comput. Phys. **235**, 52–66 (2013)
12. Zhu, S., Satravaha, P., Lu, X.: Solving linear diffusion equations with the dual reciprocity method in Laplace space. Eng. Anal. Bound. Elem. **13**(1), 1–10 (1994)
13. Grace, L.: Non-Fickian three-dimensional moisture absorption in polymeric composites: development and validation of hindered diffusion model. Ph.D Thesis, University of Oklahoma, Norman, USA, (2012)
14. Luikov, A.V.: Analytical heat diffusion theory, p. 684. Academic Press, Inc. Ltd., London (1968)
15. Carslaw, H.S., Jaeger, J.C.: Conduction of heat in solids. 2nd edn, p. 510. University Press, Oxford, New York (1959)
16. Melo, R.Q.C., Santos, W.R.G., Lima, A.G.B.: Applying the Lagmuir-type model on the water absorption in vegetable fiber reinforced polymer composites: A finite-volume approach. In: XXXVIII Iberian Latin-American Congress on Computational Methods in Engineering, Florianópolis, Brazil. (2017)
17. Patankar, S.V.: Numerical heat transfer and fluid flow. Hemisphere Publishing Corporation, New York (1980)
18. Maliska, C.R.: Computational heat transfer and fluid mechanics. LTC, Rio de Janeiro (2004).(In Portuguese)
19. Silva, C.J.: Water absorption in composite materials of vegetal fiber: modeling and simulation via CFX. Master Dissertation in Mechanical Engineering, Federal University of Campina Grande, Brazil (2014) (In Portuguese)
20. Nóbrega, M.M.S., Cavalcanti, W.S., Carvalho, L.H., Lima, A.G.B.: Water absorption in unsaturated polyester composites reinforced with caroá fiber fabrics: modeling and simulation. Mat. -wiss. u.Werkstofftech. 41(5), 300–305 (2010)
21. Melo, R.Q.C., Fook, M.V.L., Lima, A.G.B.: Non-fickian moisture transport in vegetable-fiber-reinforced polymer composites using a Langmuir-type model. Polymers 12, 2503 (2020)
22. Santos, W.R.G., Melo, R.Q.C., Correia, B.R.B., Magalhães, H.L.F., Cabral, E.M., Figueiredo, M.J., Lima, A.G.B.: Water absorption in vegetable fiber-reinforced polymer composites: A

three-dimensional investigation using the Langmuir-type model. Defect Diffus For **399**, 164–170 (2020)
23. Santos, W.R.G., Brito, M.K.T., Lima, A.G.B.: Study of the moisture absorption in polymer composites reinforced with vegetal fiber using Langmuir's model. Mater. Res. 22, e20180848 (2019)
24. Brito, M.K.T., Santos, W.R.G., Correia, B.R.B., Queiroz, R.A., Tavares, F.V.S., Oliveira Neto, G.L., Lima, A.G.B.: Moisture absorption in polymer composites reinforced with vegetable fiber: a three-dimensional investigation via Langmuir model. Polymers 11, 1847 (2019)
25. Santos, W.R.G.: Heat and mass transfer in polymeric composites reinforced by vegetable fibers: advanced modeling and simulation. Campina Grande: Doctoral Thesis in Process Engineering, Federal University of Campina Grande, Campina Grande, Brazil, (2019)
26. Sanchez, E.M., Cavani, C.S., Leal, C.V., Sanchez, C.G.: Composites of unsaturated polyester resin with sugarcane bagasse: influence of fiber treatment on properties. Polymer **20**(3), 194–200 (2010)